On the Courant-Friedrichs-Lewy condition for numerical solvers of the coagulation equation

Guillaume Laibe, Maxime Lombart

Monthly Notices of the ROYAL ASTRONOMICAL SOCIETY

MNRAS **510,** 5220–5225 (2022) https://doi.org/10.1093/mnras/stab3499
Advance Access publication 2021 December 4

On the Courant–Friedrichs–Lewy condition for numerical solvers of the coagulation equation

Guillaume Laibe[1,2]★ and Maxime Lombart[1]

[1]*Univ Lyon, Univ Lyon1, Ens de Lyon, CNRS, Centre de Recherche Astrophysique de Lyon UMR5574, F-69230 Saint-Genis-Laval, France*
[2]*Institut Universitaire de France, France*

Accepted 2021 September 17. Received 2021 September 1; in original form 2021 June 25

ABSTRACT

Evolving the size distribution of solid aggregates challenges simulations of young stellar objects. Among other difficulties, generic formulae for stability conditions of explicit solvers provide severe constraints when integrating the coagulation equation for astrophysical objects. Recent numerical experiments have reported that these generic conditions may be much too stringent. By analysing the coagulation equation in the Laplace space, we explain why this is indeed the case and provide a novel stability condition that avoids time oversampling.

Key words: methods: numerical – dust, extinction.

1 INTRODUCTION

The coagulation equation – also called the Smoluchowski equation – is one of the fundamental equations of physics, since it describes mass conservation for a distribution of interacting particles (Banasiak, Lamb & Laurencot 2019). It plays a central role in the formation of planets, since solid bodies, originating from the interstellar medium, have to grow over 30 orders of magnitude in mass to form cores of planets (Chiang & Youdin 2010). As they grow, grains undergo a complex interplay between coagulation and dynamics since dust/gas interaction depends strongly on the size of the dust grains (Testi et al. 2014), hence the necessity of performing three-dimensional simulations of young stellar objects that integrate the coagulation equation in a self-consistent manner (Haworth et al. 2016). However, this task was long thought to be computationally prohibitive, since no hydrodynamical code could handle the large number of dust bins required to solve for the coagulation equation without overdiffusion. Recently, Lombart & Laibe (2021) showed that overdiffusivity at small bin numbers could be overcome by the means of a discontinuous Galerkine algorithm of high spatial order (Liu, Gröpler & Warnecke 2019). Still, to maintain practical performance, the coagulation solver should not be called too often per hydrodynamical time-step (Drążkowska, Windmark & Dullemond 2014; Drążkowska et al. 2019). Stability condition for explicit schemes has been studied since the very beginning of the numerical study of the coagulation equation (Filbet & Laurencot 2004; Dullemond & Dominik 2005; Gabriel & Tine 2010; Forestier-Coste & Mancini 2012; Liu et al. 2019). Time-stepping is set by the so-called Courant–Friedrichs–Lewy condition (or the CFL condition; Courant, Friedrichs & Lewy 1928), which is thought to become drastically small for planet formation, making the solver of no practical use. An alternate solution consists of using implicit solvers, an approach successfully used for fragmentation (Mahoney & Ramkrishna 2002; Jacobson 2005; Sandu 2006; Brauer, Dullemond & Henning 2008; Birnstiel, Dullemond & Brauer 2010), but at the cost of heavy linear algebra operations that increase with the order of the scheme.

Remarkably, Liu et al. (2019) noticed that his numerical solver was numerically stable for a time-step that is orders of magnitude larger than the one given by the generic CFL condition (Section 2). 'Only for $\Delta t \leq 0.005$ do we observe a stable solution without using a reconstruction step. This is a significant restriction. With the use of the scaling limiter presented above, we observe that no negative values are generated by the scheme and therefore the solution remains stable, even when raising the time-step to $\Delta t = 1$.' The real CFL condition should therefore be less draconian than the one generically used. Finding it is the goal of this study.

The generic CFL criterion for hyperbolic equations has been proven not only to ensure stability, but also to strict positivity of the mass distribution (Filbet & Laurencot 2004). In a discontinuous Galerkine solver, positivity is instead enforced with a slope limiter, associated with an Strong Stability Preserving (SSP) integrator. Unlocking this positivity constrain ensures that numerical stability is actually set by the shortest physical time in which mass transfers through the dust distribution. A high-order scheme then ensures accuracy even when integration is performed with large time-steps. Since the coagulation flux is expressed as a double integral over the mass distribution, this time should result from integral considerations over the mass distribution, an information encoded in the Laplace transform of the Smoluchowski equation. Looking at the physical time-scales that appear when decomposing the mass distribution into decaying exponentials reveals an alternate and less stringent CFL condition than the ones previously used (Section 3). We validate these findings by testing this condition back in the mass space with the solver of Lombart & Laibe (2021). In this study, we focus on constant and additive kernels, since they can be associated with analytical solutions that are the most relevant for planet formation.

★ E-mail: glaibe@ens-lyon.fr

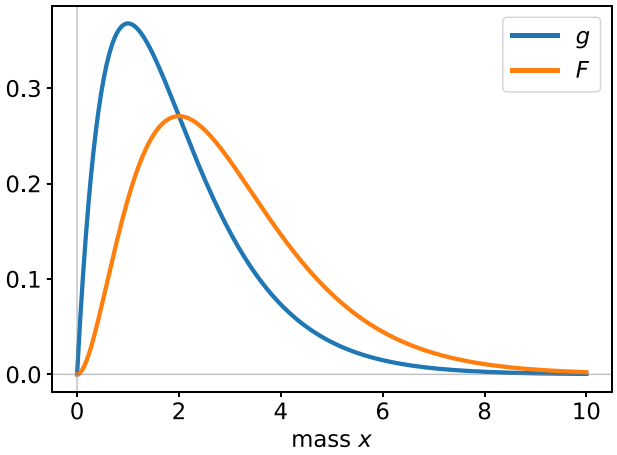

Figure 1. Analytical solution for the mass density distribution g and the coagulation flux F for $K = 1$ and $f(x, 0) = \mathrm{e}^{-x}$ at $t = 1$. The maximum of g does not correspond to the maximum of F.

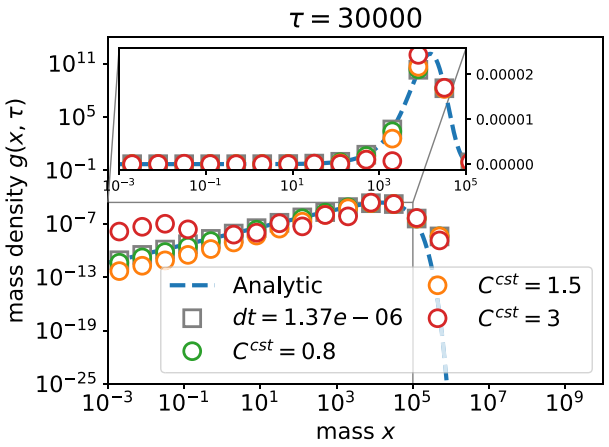

Figure 2. Numerical integration of the Smoluchowski equation with a discontinuous Galerkine scheme of order 2. Solutions are displayed in log–log scale for the main plot and lin–log scale when zooming-in close to the maximum. Grey squares correspond to the generic stability condition equation (4) (initially, $\Delta t \simeq 1 \times 10^{-6}$). Green, orange, and red circles correspond to $\Delta t \simeq 0.8\Delta t_{\mathrm{CFL}}$, $\Delta t \simeq 1.5\Delta t_{\mathrm{CFL}}$, and $\Delta t \simeq 3\Delta t_{\mathrm{CFL}}$, respectively, where $\Delta t_{\mathrm{CFL}} = M_0^{-1}$ from equation (10). No oscillations develop when the novel CFL condition is satisfied (green), and numerical integration remains stable. Blue dashed line: analytical solution.

2 SMOLUCHOWSKI EQUATION

The Smoluchowski equation is a mean-field, non-linear, integro-differential equation that models mass conservation along a binary collisional process (Smoluchowski 1916). The evolution of the number density of particles per unit mass f is given by

$$\frac{\partial f}{\partial t} = \frac{1}{2}\int_0^x K(y, x-y)\, f(y)\, f(x-y)\,\mathrm{d}y - f(x)\int_0^\infty K(y, x)\, f(y)\,\mathrm{d}y, \tag{1}$$

where the kernel $K(x, y)$ is a symmetric function that gives the collisional rate between particles of masses x and y. The conservative form of equation (1) is

$$\frac{\partial g}{\partial t} + \frac{\partial F[g]}{\partial x} = 0, \tag{2}$$

where $g \equiv xf$ is the mass density distribution per unit mass, and

$$F(x) = \int_0^x \int_{x-u}^\infty K(u, v)\, g(u)\, \frac{g(v)}{v}\mathrm{d}u\mathrm{d}v \tag{3}$$

is the coagulation flux (Tanaka, Inaba & Nakazawa 1996). The usual CFL condition for conservative equations of the form Eq. 2 is

$$\frac{\Delta t}{\Delta x}\max_g\left|\frac{\partial F}{\partial g}\right| \lesssim 1. \tag{4}$$

For the Smoluchowski equation, the condition given by equation (4) may be stringent when considering local individual contribution to the flux of each mass bin. Fig. 1 shows indeed that the quantity $|\partial F/\partial g|^{-1}$ can become extremely small, since small increments δg may become very small at the location of the maximum of g, while δF remains finite. A physical stability condition should instead consider the cumulated contributions of every bins to the local flux, accounting for the contribution of the mass distribution that generates the flux in the mass space. A natural tool to handle these effects consists of determining a stability condition for the time-step in the dual Laplace space. We therefore introduce the Laplace transform $\hat{f}(p, t) \equiv \int_0^\infty \mathrm{e}^{-px} f(x, t)\,\mathrm{d}x$ of the number density distribution.

3 PHYSICAL TIME-STEPPING

3.1 Constant kernel

We first consider the constant kernel $K = 1$. Taking the Laplace transform of equation (1) gives

$$\partial_t \hat{f} + M_0(t)\,\hat{f} - \frac{1}{2}\hat{f}^2 = 0, \tag{5}$$

where, for the unit kernel, $M_0(t) = (1 + t/2)^{-1}$ (Müller 1928). We first note that

$$0 \le \hat{f}(p, t) \le \hat{f}(0, t) = M_0(t). \tag{6}$$

Equation (6) shows that the non-linear contribution lightens the linear term in equation (5). Discretizing equation (5) with a forward Euler scheme and performing a linear stability analysis of the form $\hat{f}^n = \hat{f}_0^n + \epsilon^n$ gives

$$\frac{\epsilon^{n+1} - \epsilon^n}{\Delta t} + M_0^n \epsilon^n = \hat{f}_0^n \epsilon^n, \tag{7}$$

i.e.

$$\epsilon^{n+1} = \epsilon^n\left[1 - \Delta t\left(M_0^n - \hat{f}_0^n\right)\right]. \tag{8}$$

Stability of the scheme is obtained at any time from the sufficient condition $\Delta t \le \min\left(M_0^n - \hat{f}_0^n\right)^{-1}$. A stringent majorant for Δt is therefore

$$\Delta t \le 1/M_0^n. \tag{9}$$

A stability condition for an explicit scheme is therefore set by the typical time-scale M_0^{-1} of the linear term, as one would expect from the evolution of the moments of the equation (Banasiak et al. 2019). Generally, the novel stability condition should be weighted by a safety coefficient C^{cst}

$$\Delta t \le \frac{C^{\mathrm{cst}}}{M_0^n} = \mathcal{O}\left(M_0^{-1}\right). \tag{10}$$

This basal Von Neumann analysis is checked by integrating equation (5) within the Laplace space with a forward Euler scheme (Fig. B1). Numerical results are compared to an analytical solution of equation (5) (integrating only with respect to time in this particular case)

$$\hat{f}\,(p,t) = \frac{2}{2+t}, \tag{11}$$

and $C^{\rm cst} = 1$. Numerical results are in excellent agreement with the theoretical analysis. The real test consists of testing the condition equation (10) in the mass space. We therefore solve the Smoluchowski equation with the algorithm of Lombart & Laibe (2021). We use nine orders of magnitude in mass and $n = 15$ log-spaced bins to mimic the challenging integration conditions encountered in practice. We find numerical stability for the same exact condition (Fig. 2). For $\Delta t \leq \Delta t_{\rm CFL}$, the numerical integration follows the analytical solution with an unexpected accuracy even close to marginal stability, confirming the observation of Liu et al. (2019). When $\Delta t \geq \Delta t_{\rm CFL}$, numerical solution breaks strongly at small masses. In practice, the constant $C^{\rm cst}$ should be chosen to provide the desired trade-off between computational efficiency and numerical accuracy. We verified the criterion on distributions with other values of M_0.

3.2 Additive kernel

Let us now consider the additive kernel $K = x + y$. For this kernel, M_1 is constant and $\mathrm{d}M_0/\mathrm{d}t = -M_1 M_0$ (Golovin 1963); hence,

$$M_0\,(t) = M_0^{\rm i}\,\mathrm{e}^{-M_1 t}. \tag{12}$$

The Laplace transform of equation (1) is

$$\partial_t \hat{f} = \left[M_0\,(t) - \hat{f}\right]\partial_p \hat{f} - M_1 \hat{f}. \tag{13}$$

Contrary to the constant case, the contribution of the term $\left[M_0\,(t) - \hat{f}\right]\partial_p \hat{f}$ reinforces the contribution of the term $-M_1\hat{f}$ and contributes to numerical stability. The strategy of analysis now consists in looking at the characteristics of the problem, to show the existence of a real number $C > 0$ that does not depend on p, such that $-C \leq \partial_t \ln \hat{f} \leq 0$. As such, $\hat{f}$ decreases slower than a decaying exponential for which the stability condition is known. Equation (13) becomes

$$\left(\partial_t \hat{f}, \partial_p \hat{f}, -1\right)\cdot\left(1,\, \hat{f} - M_0\,(t)\,, -M_1\hat{f}\right) = 0. \tag{14}$$

Equation (14) is solved by a method of characteristics by setting $t = t(r,s)$, $p = p(r,s)$, $u = u\,(r,s) \equiv \hat{f}\,(t,\,p)$, and $u\,(t\,(0,s)\,,\,p\,(0,s)) = \hat{f}_0\,(s)$, following Banasiak et al. (2019). One has

$$\partial_r t = 1, \qquad t\,(0,s) = 0, \tag{15}$$

$$\partial_r p = u - M_0\,(r)\,, \qquad p\,(0,s) = s, \tag{16}$$

$$\partial_r u = -M_1 u, \qquad u\,(0,s) = \hat{f}_0\,(s)\,. \tag{17}$$

Equation (15) gives $t(r,\,s) = r$ and equation (17) gives $u\,(r,s) = \hat{f}_0\,(s)\,\mathrm{e}^{-M_1 r}$. Integrating equation (12), solving for equation (16) gives

$$p\,(r,s) = s + \frac{\left(\hat{f}_0\,(s) - M_0^{\rm i}\right)}{M_1}\left(1 - \mathrm{e}^{-M_1 r}\right). \tag{18}$$

Consider now $z(r,\,p)$, the implicit solution of equation (18) where r and p are seen as two independent variables, i.e.

$$p = z\,(r,\,p) + \frac{\left(\hat{f}_0\,(z\,(r,\,p)) - M_0^{\rm i}\right)}{M_1}\left(1 - \mathrm{e}^{-M_1 r}\right). \tag{19}$$

Then, $\hat{f}\,(t\,(r,s)\,,\,p\,(r,s)) = u\,(t,\,s = z\,(t,\,p))$, and $\hat{f}\,(t,\,p)$ is expressed in the implicit form $\hat{f}\,(t,\,p) = \hat{f}_0\,(z\,(t,\,p))\,\mathrm{e}^{-M_1 t}$. Deriving with respect to time gives

$$\partial_t \ln \hat{f} = -M_1 + \partial_t z\,(t,\,p)\,\frac{\hat{f}_0'\,(z\,(t,\,p))}{\hat{f}_0\,(z\,(t,\,p))}, \tag{20}$$

where we have denoted for convenience $\hat{f}_0'\,(p) = \partial_p \hat{f}_0\,(p)$. Differentiating equation (18) with respect to r gives

$$\frac{\partial z}{\partial r} = M_1\,\frac{\left(M_0^i - \hat{f}_0\right)\mathrm{e}^{-M_1 r}}{M_1 + \hat{f}_0'\left(1 - \mathrm{e}^{-M_1 r}\right)}. \tag{21}$$

The identity $\hat{f}_0'\,(p) = -\int_0^\infty x\mathrm{e}^{-px} f\,(x)\,\mathrm{d}x$ ensures that

$$0 \leq \partial_t z \leq M_1\,\frac{M_0^i - \hat{f}_0}{M_1 + \hat{f}_0'}, \tag{22}$$

and that for any p,

$$0 \geq \partial_t \ln \hat{f} \geq -M_1\,(1 + T\,(p))\,, \tag{23}$$

where $T(p) \geq 0$ is given by

$$T\,(p) \equiv \frac{\int_0^\infty x\mathrm{e}^{-px} f_0\,(x)\,\mathrm{d}x}{\int_0^\infty \mathrm{e}^{-px} f_0\,(x)\,\mathrm{d}x}\,\frac{\int_0^\infty \left(1 - \mathrm{e}^{-px}\right) f_0\,(x)\,\mathrm{d}x}{\int_0^\infty (1 - \mathrm{e}^{-px})\,x f_0\,(x)\,\mathrm{d}x}. \tag{24}$$

Therefore, the physical solution decays more slowly than an envelope with exponential decay and is associated with the stability condition

$$\Delta t \lesssim \frac{C^{\rm add}}{M_1\left(1 + \sup\limits_p T\,[f_0]\right)}. \tag{25}$$

In Appendix A, we prove that $T(p) \leq 1$, allowing us to write the condition of equation (25)

$$\Delta t \lesssim \frac{C^{\rm add}}{2M_1} = \mathcal{O}\left(M_1^{-1}\right). \tag{26}$$

A refined criterion can be obtained when $T\left[\hat{f}_0\right]$ is actually a decreasing function of p. In this case, $T\,(p) \leq T\,(0) = M_1^2/M_0^{\rm i} M_2^{\rm i}$, which would provide the refined stability condition

$$\Delta t \lesssim \frac{C^{\rm add}}{M_1\left(1 + \frac{M_1^2}{M_0^{\rm i} M_2^{\rm i}}\right)}. \tag{27}$$

We obtain excellent agreement for the conditions given by equations (25)–(27) in the Laplace space (Fig. B1), against a numerical solution obtained at high resolution. Fig. 3 shows very good applicability of this condition in the real space (varying M_1 gives similar results). This validates the findings of Liu et al. (2019). For example, a factor of $\sim$10 in processing time is gained with the novel condition.

The term $\sup_p T\,[f_0]$ of equation (25) is the mathematical consequence of the fact that the contribution of $\left[M_0\,(t) - \hat{f}\right]\partial_p \hat{f}$ reinforces the one of $-M_1\hat{f}$ in equation (13). Finding this correction to be of order unity is physically consistent with fluxes of mass of similar intensities generated by the two terms of the right-hand side of equation (1). We note that the CFL condition comes from the limit $p \to 0$, which corresponds to the limit case of a constant mass distribution that is non-integrable over the mass space. Mass fluxes are indeed expected to be more intense for this distribution, since an additive kernel favours growth over the largest grains. We conjecture that this CFL condition can, alternatively, be obtained from the evolution of the moments of equation (1). The method presented here can be applied to other relevant coagulation kernels.

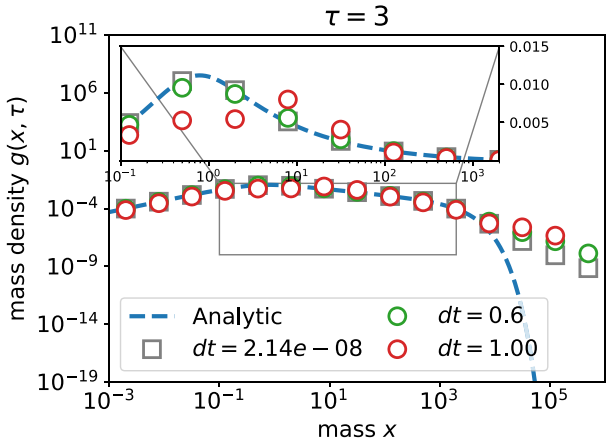

Figure 3. Numerical integration of the Smoluchowski equation with a discontinuous Galerkine scheme of order 2. Solutions are displayed in log–log scale for the main plot and lin–log scale when zooming-in close to the maximum. Grey squares correspond to the generic stability condition equation (4) (initially, $\Delta t \simeq 2 \times 10^{-8}$). Green and red circles correspond to $\Delta t \simeq 0.9\Delta t_{\rm CFL}$ and $\Delta t \simeq 1.5\Delta t_{\rm CFL}$, respectively, where $\Delta t_{\rm CFL} = 2/3$ from equation (27). No oscillations develop when the novel CFL condition is satisfied (green), and numerical integration remains stable. Blue dashed line: analytical solution.

4 CONCLUSION

In this study, we revisit the derivation of the stability condition for explicit numerical solvers of the Smoluchowski equation. Generic formulae are too stringent since they also ensure positivity. Enforcing positivity by some alternate way (e.g. with a slope limiter associated with an SSP integrator) allows to improve stability condition by several orders of magnitude. Novel conditions that involve moments of the mass distribution – $\Delta t_{\rm CFL} \sim M_0^{-1}$ for the constant kernel and $\Delta t_{\rm CFL} \sim M_1^{-1}$ for the additive kernel – are obtained by analysing dual problems in the Laplace space, to account for the non-locality of the coagulation equation and its different responses to different dust distributions. Numerical simulations are in excellent agreement with the theory and validate our novel CFL condition, confirming the observations of Liu et al. (2019).

ACKNOWLEDGEMENTS

GL acknowledges funding from the ERC CoG project PODCAST no. 864965. This project has received funding from the European Union's Horizon 2020 research and innovation programme under the Marie Skłodowska-Curie Actions grant agreement no. 823823. This project was partly supported by the IDEXLyon project (contract nANR-16-IDEX-0005) under the auspices University of Lyon. We acknowledge financial support from the national programmes (PNP, PNPS, PCMI) of CNRS/INSU, CEA, and CNES, France. We thank E. Lynch for useful comments.

DATA AVAILABILITY

The data and supplementary material underlying this article are available in the repository 'growth' on GitHub at https://github.com/mlombart/growth.git. Figures can be reproduced following the file `README.md`. The repository contains data and PYTHON scripts used to generate figures.

REFERENCES

Banasiak J., Lamb W., Laurencot P., 2019, Analytic Methods for Coagulation-Fragmentation Models, Vol. I. Chapman and Hall/CRC, p. 3
Birnstiel T., Dullemond C. P., Brauer F., 2010, A&A, 513, A79
Brauer F., Dullemond C. P., Henning T., 2008, A&A, 480, 859
Chiang E., Youdin A. N., 2010, Annu. Rev. Earth Planet. Sci., 38, 493
Courant R., Friedrichs K., Lewy H., 1928, Math. Ann., 100, 32
Drążkowska J., Windmark F., Dullemond C. P., 2014, A&A, 567, A38
Drążkowska J., Li S., Birnstiel T., Stammler S. M., Li H., 2019, ApJ, 885, 91
Dullemond C. P., Dominik C., 2005, A&A, 434, 971
Filbet F., Laurencot P., 2004, SIAM J. Sci. Comput., 25, 2004
Forestier-Coste L., Mancini S., 2012, SIAM J. Sci. Comput., 34, B840
Gabriel P., Tine L. M., 2010, ESAIM Proc., 30, 53
Golovin A., 1963, Izv. Geophys. Ser., 5, 482
Haworth T. J. et al., 2016, Publ. Astron. Soc. Aust., 33, e053
Jacobson M. Z., 2005, Fundam. Atmos. Model. Cambridge University Press
Liu H., Gröpler R., Warnecke G., 2019, SIAM J. Sci. Comput., 41, B448
Lombart M., Laibe G., 2021, MNRAS, 501, 4298
Mahoney A. W., Ramkrishna D., 2002, Chem. Eng. Sci., 57, 1107
Müller H., 1928, Fortschr. Kolloide Polym., 27, 223
Sandu A., 2006, Aerosol Sci. Technol., 40, 261
Smoluchowski M. V., 1916, Z. Phys., 17, 557
Tanaka H., Inaba S., Nakazawa K., 1996, Icarus, 123, 450
Testi L. et al., 2014, Protostars and Planets VI. Univ. Arizona Press, Tucson, AZ, p. 339
Yang Z.-H., Tian J., 2017, J. Inequal. Appl., 317

APPENDIX A: BOUNDING OF T

Following Yang & Tian (2017), let denote

$$T(p) \equiv \underbrace{\frac{\int_0^\infty x\mathrm{e}^{-px} f_0(x)\,\mathrm{d}x}{\int_0^\infty \mathrm{e}^{-px} f_0(x)\,\mathrm{d}x}}_{T_1 \equiv I_1/I_2} \underbrace{\frac{\int_0^\infty \left(1-\mathrm{e}^{-px}\right) f_0(x)\,\mathrm{d}x}{\int_0^\infty (1-\mathrm{e}^{-px})\, x f_0(x)\,\mathrm{d}x}}_{T_2 \equiv I_3/I_4}. \tag{A1}$$

Deriving T_1 with respect to p and symmetrizing $x \leftrightarrow y$ gives

$$I_2(p)^2 \frac{\mathrm{d}T_1[f](p)}{\mathrm{d}p} \equiv -\left\{\left(\int_0^\infty \mathrm{e}^{-px} f(x)\,\mathrm{d}x\right)\left(\int_0^\infty \mathrm{e}^{-px} x^2 f(x)\,\mathrm{d}x\right) - \left(\int_0^\infty \mathrm{e}^{-px} x f(x)\,\mathrm{d}x\right)^2\right\} \tag{A2}$$

$$= -\left\{\int_0^\infty\int_0^\infty \mathrm{d}x\mathrm{d}y\, \mathrm{e}^{-px}\mathrm{e}^{-py} f(x) f(y)\, y^2 - \int_0^\infty\int_0^\infty \mathrm{d}x\mathrm{d}y\, \mathrm{e}^{-px}\mathrm{e}^{-py} f(x) f(y)\, xy\right\} \tag{A3}$$

$$= -\left\{\int_0^\infty\int_0^\infty \mathrm{d}x\mathrm{d}y\, \mathrm{e}^{-px}\mathrm{e}^{-py} f(x) f(y)\, \frac{\left(x^2+y^2\right)}{2} - \int_0^\infty\int_0^\infty \mathrm{d}x\mathrm{d}y\, \mathrm{e}^{-px}\mathrm{e}^{-py} f(x) f(y)\, xy\right\} \tag{A4}$$

$$= -\frac{1}{2}\int_0^\infty\int_0^\infty \mathrm{d}x\mathrm{d}y\, \mathrm{e}^{-px}\mathrm{e}^{-py} f(x) f(y)(x-y)^2 < 0. \tag{A5}$$

Hence, $T_1[f]$ is a decreasing function for any f. As such,

$$T_1[f_0](p) \leq T_1[f_0](0) = \frac{M_1}{M_0}. \tag{A6}$$

Similarly, deriving T_2 with respect to p gives

$$I_4(p)^2 \frac{\mathrm{d}T_2[f](p)}{\mathrm{d}p} \equiv \left\{\left(\int_0^\infty \left(1-\mathrm{e}^{-px}\right) x f(x)\,\mathrm{d}x\right)\left(\int_0^\infty x\mathrm{e}^{-px} f(x)\,\mathrm{d}x\right)\right.$$
$$\left. - \left(\int_0^\infty x^2\mathrm{e}^{-px} f(x)\,\mathrm{d}x\right)\left(\int_0^\infty \left(1-\mathrm{e}^{-px}\right) f(x)\,\mathrm{d}x\right)\right\} \tag{A7}$$

$$= \left\{\int_0^\infty\int_0^\infty \mathrm{d}x\mathrm{d}y\, f(x) f(y)\, xy\left(1-\mathrm{e}^{-px}\right)\mathrm{e}^{-py} - \int_0^\infty\int_0^\infty \mathrm{d}x\mathrm{d}y\, f(x) f(y)\, x^2\mathrm{e}^{-px}\left(1-\mathrm{e}^{-py}\right)\right\} \tag{A8}$$

$$= \frac{1}{2}\left\{\int_0^\infty\int_0^\infty \mathrm{d}x\mathrm{d}y\, f(x) f(y) \underbrace{(y-x)\left[x\mathrm{e}^{-px}\left(1-\mathrm{e}^{-py}\right) - y\mathrm{e}^{-py}\left(1-\mathrm{e}^{-px}\right)\right]}_{\geq 0}\right\}. \tag{A9}$$

Hence, $T_2[f]$ is strictly increasing function for any f,

$$T_2[f_0](p) \leq T_2[f_0](\infty) = \frac{M_0}{M_1}. \tag{A10}$$

Finally, $T(p) = T_1(p)T_2(p) \leq 1$.

APPENDIX B: STABILITY CONDITION IN THE LAPLACE SPACE

Fig. B1 shows the validity of the stability conditions obtained for the numerical integration of $\hat{f}$ (Laplace space) in Section 3.

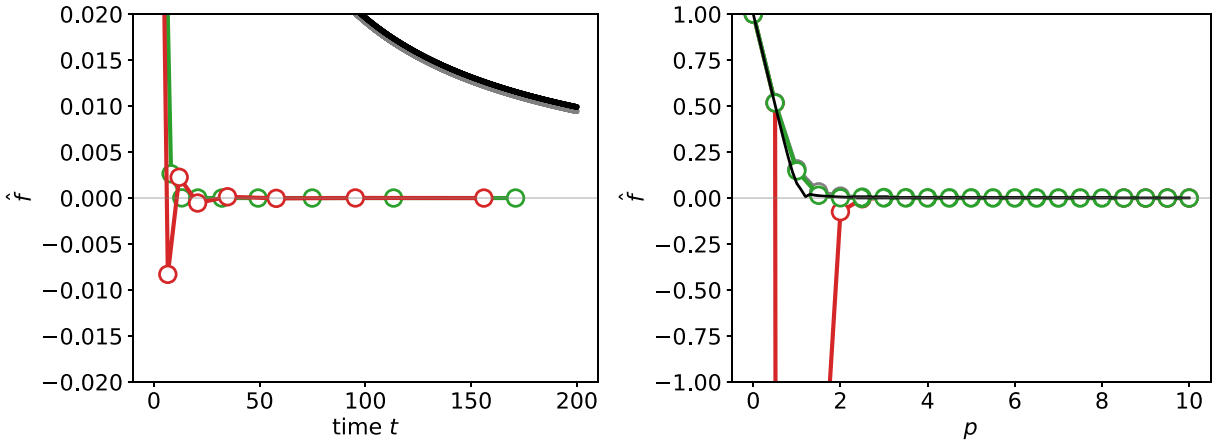

Figure B1. Left: Numerical solution of equation (5) obtained with a first-order Euler scheme. Small grey, large green, and large red circles correspond to $\Delta t = 10^{-3}\,\Delta t_{\rm CFL}$, $\Delta t = 1\Delta t_{\rm CFL}$, and $\Delta t = 1.25\Delta t_{\rm CFL}$, respectively, where $\Delta t_{\rm CFL}$ is given by equation (25) ($C^{\rm cst} = 1$). Δt varies with time. Black solid line: analytical solution. Right: Numerical solution of equation (13) obtained with a first-order upwind scheme, under the condition $\hat{f}\,(0, t) = 1$ with 20 grid points. Grey, large green, and large red circles correspond to $\Delta t \simeq 0.09\Delta t_{\rm CFL}$, $\Delta t \simeq 0.83\Delta t_{\rm CFL}$, and $\Delta t \simeq 1.07\Delta t_{\rm CFL}$, respectively, where $\Delta t_{\rm CFL} = 2/3$ from equation (27) ($C^{\rm add} = 1$). Black solid line: analytical solution (a better sampling in mass makes the numerical solution closer to the analytical solution).

This paper has been typeset from a TEX/LATEX file prepared by the author.